Cardiovascular risks impact human brain *N*-acetylaspartate in regionally specific patterns

Joshua Chiappelli[a,1,2], Laura M. Rowland[a,1,2], S. Andrea Wijtenburg[a], Hongji Chen[a], Andrew A. Maudsley[b], Sulaiman Sheriff[b], Shuo Chen[a], Anya Savransky[a], Wyatt Marshall[a], Meghann C. Ryan[a], Heather A. Bruce[a], Alan R. Shuldiner[c], Braxton D. Mitchell[c,d], Peter Kochunov[a], and L. Elliot Hong[a]

[a]Maryland Psychiatric Research Center, Department of Psychiatry, University of Maryland School of Medicine, Baltimore, MD 21228; [b]Department of Radiology, University of Miami School of Medicine, Miami, FL 33136; [c]Department of Medicine, University of Maryland School of Medicine, Baltimore, MD 21201; and [d]Geriatrics Research and Education Clinical Center, Baltimore Veterans Administration Medical Center, Baltimore, MD 21201

Cardiovascular risk factors such as dyslipidemia and hypertension increase the risk for white matter pathology and cognitive decline. We hypothesize that white matter levels of *N*-acetylaspartate (NAA), a chemical involved in the metabolic pathway for myelin lipid synthesis, could serve as a biomarker that tracks the influence of cardiovascular risk factors on white matter prior to emergence of clinical changes. To test this, we measured levels of NAA across white matter and gray matter in the brain using echo planar spectroscopic imaging (EPSI) in 163 individuals and examined the relationship of regional NAA levels and cardiovascular risk factors as indexed by the Framingham Cardiovascular Risk Score (FCVRS). NAA was strongly and negatively correlated with FCVRS across the brain, but, after accounting for age and sex, the association was found primarily in white matter regions, with additional effects found in the thalamus, hippocampus, and cingulate gyrus. FCVRS was also negatively correlated with creatine levels, again primarily in white matter. The results suggest that cardiovascular risks are related to neurochemistry with a predominantly white matter pattern and some subcortical and cortical gray matter involvement. NAA mapping of the brain may provide early surveillance for the potential subclinical impact of cardiovascular and metabolic risk factors on the brain.

white matter | hypertension | neurochemistry | creatine

Longitudinal studies have found that cardiovascular and metabolic risk factors such as hypertension and dyslipidemia in early and middle adulthood are predictive of later cognitive decline and development of neurodegenerative disorders such as Alzheimer's disease (1–5). The association of cardio-metabolic risk factors and brain-related clinical outcomes may be mediated by the effects of these risk factors on white matter structure (1, 6). Previously, we found that peripheral adiposity was correlated with brain white matter microstructure as measured with diffusion-weighted imaging (7). Here we investigate the possibility that neurochemistry assessed with proton magnetic resonance spectroscopy (MRS) can provide a more proximal biomarker for the association of cardio-metabolic risk to white matter, with a focus on *N*-acetylaspartate (NAA) and glutamate and glutamine (Glx). NAA is an abundant neurometabolite produced in mitochondria and stored largely in neuronal bodies and their axons in the brain. Levels of NAA are sensitive to a range of pathologies resulting in neuronal loss or damage, and thus levels of NAA are interpreted as a nonspecific marker of neuronal health (8, 9). In white matter, the majority of NAA is located in axons, thought to reflect NAA's roles in maintaining the axonal-glial system (8, 10, 11) and in supporting myelin synthesis (12). NAA decreases with age and has been investigated as a potential early marker for Alzheimer's disease (13–15).

Glutamate is an abundant amino acid in the brain and also serves as a neurotransmitter; maintenance of neuronal glutamate levels requires intensive metabolic support (16). Age-related decline in Glx is well documented using MRS, and decreased levels

have been observed in Alzheimer's disease and mild cognitive impairment (17–19). We hypothesize that cardiovascular risk factors may impact the brain in part through neurometabolites including NAA and Glx. Support for this hypothesis could provide early biomarkers for further mechanistic studies on the contribution of cardiovascular risks to cognitive decline and development of neurodegenerative disorders (3, 5).

Several previous studies have found NAA levels to be associated with measures of general physical health, that is, NAA levels are higher in individuals with good aerobic fitness, and lower in individuals with a high body-mass index or who smoke cigarettes (20–22). Moreover, previous studies on NAA and Glx associations with cardiovascular risk factors mostly measured neurochemistry in a limited number of brain regions. To improve the anatomic specificity of NAA and Glx levels as intermediary biomarkers for the effects of cardiovascular risk factors, we employed 3-dimensional (3D) echo-planar spectroscopic imaging (EPSI) that can reliably detect NAA, Glx, and several other metabolites across the whole brain in high resolution (23–26). EPSI is a method for acquiring 3D spectroscopic data in a shorter period of time compared to previous methods; details of this

Significance

We used a 3-dimensional whole-brain spectroscopic imaging technique to determine the relationship of the Framingham Cardiovascular Risk Score (FCVRS) to neurochemistry in a sample of Amish participants without neurologic or psychiatric disorders. Cardiovascular risk scores were inversely associated with *N*-acetylaspartate (NAA), especially in white matter regions. As NAA is a marker for neuronal integrity and serves as a reservoir for precursors to myelin lipid synthesis, the relationship to FCVRS implicates reduced NAA as a potential early marker and mechanistic clue for the contribution of cardiovascular risk factors to cognitive decline and neurodegenerative disorders.

MEDICAL SCIENCES

www.manaraa.com

method and possible applications are available in recent reviews (27, 28). In previous studies, EPSI has been successfully applied to study a large sample (25), analyzed using an advanced post-processing pipeline (24), and demonstrated to have excellent reproducibility at a short echo time (TE) similar to the one used in this study (29). Reliability and validity of EPSI measurements have previously been demonstrated using phantoms and by comparison of single voxel MRS and EPSI (30, 31).

We assessed cardiovascular risks using the Framingham Cardiovascular Risk Factor Score (FCVRS), a widely used and validated index that summarizes risk factors from elevated cholesterol, hypertension, and diabetes mellitus in addition to age and male sex (32). We tested the hypothesis that FCVRS would be associated with NAA and Glx in a sample of individuals from the Old Order Amish and Mennonite (OOA/M) population. This sample is uniquely suited for this research due to the relative genetic and environmental homogeneity in this population. They are all Caucasian, share a traditional rural upbringing, similar educational levels, and, due to strong cultural prohibitions, have low rates of use of alcohol, tobacco, and other drugs (33); thus, factors that could confound cardiometabolic and brain-imaging biomarker research in the general population are reduced in this population.

Results

Relationship of Regional NAA to Cardiovascular Risks. NAA was significantly related to FCVRS in 18 regions (Fig. 2A and Table 1). Seventeen regions showed inverse associations between their NAA levels and FCVRS, primarily in white matter regions but also including the thalamus, hippocampus, and cingulate gyrus. Examples of prominent associations include the left anterior corona radiata (Fig. 2C) and right hippocampus (Fig. 2D). To account for potential inflammatory effects, we repeated this analysis by including plasma levels of C-reactive protein but found that including C-reactive protein did not substantially alter the findings (Table 1).

Relationship of NAA to FCVRS Subcomponents. To examine whether the associations between NAA and FCVRS were driven primarily by any specific subcomponents, we repeated the analyses with subcomponents including age and sex as covariates.
Total cholesterol. No regional NAA was found to have significant association with plasma total cholesterol levels after correction for multiple comparisons.
High-density lipoprotein. High-density lipoprotein (HDL) levels were positively correlated mainly with NAA in white matter regions and showed both positive and negative correlations with NAA in gray matter regions (Table 1). Specifically, HDL was positively associated with NAA in the right fusiform gyrus [β = 0.22, false discovery rate (FDR) = 0.027] and negatively associated with NAA in the left inferior occipital gyrus (β = −0.22, FDR = 0.027), although these 2 regions were not part of the gray matter regions significantly associated with FCVRS.
Systolic blood pressure. Higher systolic blood pressure was only significantly associated with lower NAA in the right hippocampus (β = −0.20, FDR = 0.024) and with higher NAA in the left superior parietal gyrus (β = 0.19, FDR = 0.024). In general, systolic blood pressure tended to be negatively correlated with NAA in white matter regions but showed a less consistent relationship with NAA in gray matter (Table 1).
Smoking. Current smokers tended to have lower NAA in white matter regions compared with nonsmokers, although no correlations were significant after correction for multiple testing (Table 1).
Hemoglobin A1c/Diabetes. Group comparisons between diabetics vs. nondiabetics were not performed as only 5 participants had diabetes. Instead, we measured hemoglobin A1c (HbA1c) in all participants and found that it was significantly and negatively correlated with NAA in 14 regions (Table 1), although only 10 of

these regions were among the regions showing significant NAA and FCVRS associations.

Relationship of FCVRS to Other Metabolites. No significant correlations between FCVRS and Glx were observed (*SI Appendix*, Table S1). To explore if FCVRS was associated with NAA specifically, we performed regression models to examine the relationship of FCVRS to other metabolites including creatine, choline-containing compounds, and myoinositol. Creatine levels were significantly and negatively associated with FCVRS in a pattern resembling findings for NAA, including 9 white matter regions and 7 gray matter regions (Fig. 2B and *SI Appendix*). No significant correlations with choline or myoinositol were found (*SI Appendix*).

NAA Levels as Mediator of the Relationship Between FCVRS and White Matter Hyperintensities. Exploratory mediation analyses focused on mediation by NAA of the relationship between age-corrected FCVRS and the white matter hyperintensity (WMH) burden quantified as the number of subcortical WMH regions and the combined WMH volume of subcortical and ependymal regions. White matter NAA was a significant mediator between FCVRS and the number (95% confidence interval [CI]: 0.155 to 0.99; $P < 0.001$) as well as the volume of WMH regions (CI 0.007 to 0.03; $P < 0.001$). Average subcortical gray matter NAA also significantly mediated the relationship between FCVRS and the number (CI: 0.169 to 0.750; $P < 0.001$) and the volume (CI: 0.005 to 0.020; $P < 0.001$) of WMH. In contrast, average cortical gray matter NAA did not significantly mediate the relationship between FCVRS and WMH (CI: −0.16 to 0.32; $P = 0.48$ for the number and CI: −0.006 to 0.01; $P = 0.60$ for the volume). Full statistical results from these models are reported in *SI Appendix*, Table S2.

Discussion

In this community sample of relatively healthy individuals with a rural lifestyle, we found that common cardiovascular risk factors were associated with lower levels of NAA, particularly in the white matter, limbic regions, and thalamus. Contrary to our hypothesis, these risk factors were not related to glutamate and glutamine independent of age and sex. However, we found that lower levels of creatine were also associated with cardiovascular risks in a pattern similar to NAA. Although a few individual components of the FCVRS were found to be correlated with NAA levels, significant associations were primarily found only with the composite score.

The relationship of cardiovascular risk factors to NAA in white matter areas is of particular interest as the acetyl group of NAA that is broken down is used for the synthesis of myelin lipids. Notably, cholesterol, which does not cross the blood–brain barrier, is a major component of the myelin sheath (34). The de novo synthesis of cholesterol in the central nervous system uses acetyl CoA as a building block. NAA is synthesized in neuronal mitochondria from aspartate and acetyl CoA; NAA is stored in axons and released to neighboring oligodendrocytes where it is broken down into asparate and acetate and the acetate group is used for lipid synthesis (12). In animal models, hypertension and metabolic abnormalities have been associated with peripheral mitochondrial abnormalities (35, 36). Therefore, the association of higher FCVRS and lower NAA could reflect impaired mitochondrial function and/or an insufficient supply of energetic precursors such as ketone bodies that are preferentially used for lipid synthesis (37, 38). Decreased levels of NAA in turn could limit the capacity for oligodendrocytes to maintain the myelin sheath, leading to vulnerability for white matter deficits with aging or additional neurological insults. Levels of NAA correlate positively with fractional anisotropy, a measure of white matter microstructure derived from diffusion tensor imaging (39–41),

Chiappelli et al.

www.manaraa.com

Table 1. Associations of *N*-acetylaspartate and cardiovascular risks as measured by the FCVRS and its subcomponents (controlling for age and sex)

Region	FCVRS model 1	FCVRS model 2	Total cholesterol	HDL	Systolic BP	Smoking	HbA1c
White matter							
L. anterior corona radiata	−0.57*	−0.56*	−0.20	−0.08	−0.14	−0.19	−0.05
R. anterior corona radiata	−0.33	−0.32	−0.02	−0.11	−0.06	−0.12	−0.16
L. posterior corona radiata	−0.38	−0.39	−0.13	0.01	−0.08	−0.15	−0.15
R. posterior corona radiata	−0.58*	−0.59*	−0.10	0.04	−0.10	−0.15	−0.17
L. superior corona radiata	−0.44*	−0.46*	−0.07	0.01	−0.07	−0.18	−0.16
R. superior corona radiata	−0.51*	−0.52*	0.00	0.03	−0.08	−0.20	−0.22*
L. cingulum	−0.40*	−0.40*	−0.12	−0.01	−0.04	−0.16	−0.18*
R. cingulum	−0.34*	−0.35*	−0.06	−0.01	−0.02	−0.10	−0.19*
L. anterior limb, internal capsule	−0.44*	−0.44*	−0.04	0.09	−0.13	−0.11	−0.16
R. anterior limb, internal capsule	−0.49*	−0.50*	−0.07	0.07	−0.15	−0.11	−0.18*
Splenium of corpus callosum	−0.54*	−0.55*	−0.10	−0.02	−0.14	−0.09	−0.18*
Body of corpus callosum	−0.44*	−0.45*	−0.03	−0.03	−0.09	−0.11	−0.22*
Genu of corpus callosum	−0.21	−0.20	−0.06	−0.06	−0.02	−0.06	0.00
L. posterior thalamic radiation	−0.21	−0.22	−0.04	−0.06	0.05	−0.02	−0.17
R. posterior thalamic radiation	−0.39*	−0.40*	−0.10	−0.02	−0.09	0.00	−0.13
L. superior longitudinal fasciculus	−0.29	−0.30	−0.16	0.03	−0.10	−0.14	−0.07
R. superior longitudinal fasciculus	−0.33	−0.34	−0.03	0.10	−0.07	−0.11	−0.15
L. external capsule	−0.24	−0.24	−0.02	0.09	−0.11	−0.05	−0.14
R. external capsule	−0.25	−0.25	−0.04	−0.02	−0.07	−0.05	−0.10
L. sagittal stratum	−0.20	−0.19	−0.13	−0.03	−0.02	0.00	−0.02
R. sagittal stratum	−0.25	−0.25	−0.03	0.08	−0.07	−0.01	−0.04
Subcortical							
L. thalamus	−0.38*	−0.39*	−0.04	0.07	−0.16	−0.04	−0.15*
R. thalamus	−0.40*	−0.42*	−0.08	0.06	−0.14	−0.08	−0.16*
L. hippocampus	−0.33*	−0.33*	−0.01	0.07	−0.11	0.04	−0.12
R. hippocampus	−0.37*	−0.38*	−0.05	0.04	−0.20*	0.07	−0.09
L. putamen	−0.15	−0.16	−0.07	0.05	−0.06	0.02	−0.01
R. putamen	−0.26	−0.26	−0.02	−0.02	−0.13	−0.07	−0.06
L. caudate	−0.28	−0.28	0.03	0.04	−0.02	−0.05	−0.20*
R. caudate	−0.26	−0.26	0.10	0.06	−0.02	−0.10	−0.22*
Cortical							
L. cingulate gyrus	−0.27*	−0.28*	−0.11	0.00	−0.01	−0.08	−0.14*
R. cingulate gyrus	−0.23*	−0.23*	−0.06	0.01	−0.01	−0.06	−0.15*
L. inferior frontal gyrus	0.02	0.01	−0.02	−0.03	0.01	−0.07	0.01
R. inferior frontal gyrus	−0.25	−0.25	−0.09	−0.01	−0.12	−0.08	−0.05
L. middle frontal gyrus	−0.23	−0.23	−0.05	−0.08	0.01	0.00	−0.13
R. middle frontal gyrus	0.02	0.02	0.10	−0.03	0.08	−0.02	−0.15
L. superior frontal gyrus	0.03	0.03	−0.03	−0.07	0.11	−0.03	−0.11
R. superior frontal gyrus	0.05	0.06	0.02	−0.05	0.10	−0.01	−0.11
L. insula	−0.18	−0.18	−0.03	0.07	−0.07	−0.04	−0.11
R. insula	−0.17	−0.17	−0.02	0.03	−0.07	0.05	−0.06
L. precentral gyrus	−0.01	−0.01	−0.03	0.01	0.05	−0.05	−0.07
R. precentral gyrus	0.01	0.01	0.02	0.04	0.08	−0.08	−0.17*
L. superior parietal gyrus	0.15	0.15	−0.06	−0.10	0.19*	−0.03	−0.04
R. superior parietal gyrus	−0.13	−0.13	−0.09	−0.04	0.08	−0.11	−0.08
L. precuneus	0.06	0.06	−0.04	−0.05	0.13	−0.04	−0.09
R. precuneus	−0.06	−0.06	−0.06	−0.04	0.11	−0.04	−0.11
L. postcentral gyrus	−0.04	−0.04	−0.08	0.05	0.08	−0.04	−0.09
R. postcentral gyrus	−0.12	−0.12	−0.04	0.02	0.08	−0.05	−0.16*
L. supramarginal gyrus	−0.10	−0.11	−0.14	−0.05	0.02	−0.04	−0.04
R. supramarginal gyrus	−0.14	−0.14	0.00	0.05	−0.01	0.02	−0.15*
L. middle temporal gyrus	0.08	0.08	−0.05	−0.10	0.10	0.02	−0.06
R. middle temporal gyrus	−0.21	−0.21	0.04	0.04	−0.05	0.09	−0.13
L. superior temporal gyrus	−0.19	−0.19	−0.06	0.01	−0.02	−0.03	−0.10
R. superior temporal gyrus	−0.14	−0.15	−0.03	0.03	−0.04	0.04	−0.09
L. cuneus	0.15	0.15	0.02	−0.07	0.09	0.01	−0.12
R. cuneus	0.05	0.04	0.06	0.00	−0.01	−0.02	−0.07
L. lingual gyrus	0.03	0.03	−0.06	−0.08	0.05	0.04	−0.07
R. lingual gyrus	0.09	0.08	0.07	0.01	−0.02	0.14	0.09
L. fusiform gyrus	−0.14	−0.14	−0.03	−0.01	−0.02	−0.07	−0.07
R. fusiform gyrus	−0.21	−0.20	0.09	0.21*	−0.03	0.05	−0.06
L. angular gyrus	0.28*	0.28*	0.02	−0.14	0.15	0.05	0.00
R. angular gyrus	−0.12	−0.12	−0.05	−0.01	0.02	−0.06	−0.11
L. inferior occipital gyrus	0.16	0.16	0.01	−0.22*	0.06	0.02	−0.02
R. inferior occipital gyrus	−0.06	−0.06	−0.09	−0.01	0.02	0.10	−0.07
L. middle occipital gyrus	0.12	0.13	−0.02	−0.08	0.12	−0.01	−0.04
R. middle occipital gyrus	0.09	0.09	−0.07	0.05	0.06	−0.06	−0.07
L. superior occipital gyrus	−0.07	−0.06	−0.07	−0.04	0.06	−0.03	−0.11
R. superior occipital gyrus	0.02	0.03	−0.05	0.00	0.03	−0.10	−0.04
Cerebellum							
L. cerebellum	−0.03	−0.04	−0.04	0.07	−0.04	−0.05	−0.01
R. cerebellum	−0.20	−0.21	−0.07	0.07	−0.10	0.02	0.08

Associations with FCVRS are given as beta values from linear regression models covarying for age and sex (model 1) and models covarying for age, sex, and plasma levels of C-reactive protein (CRP) (model 2). All associations for subcomponents are beta values from regression models with age and sex as covariates. BP, blood pressure. L, left. R, right.
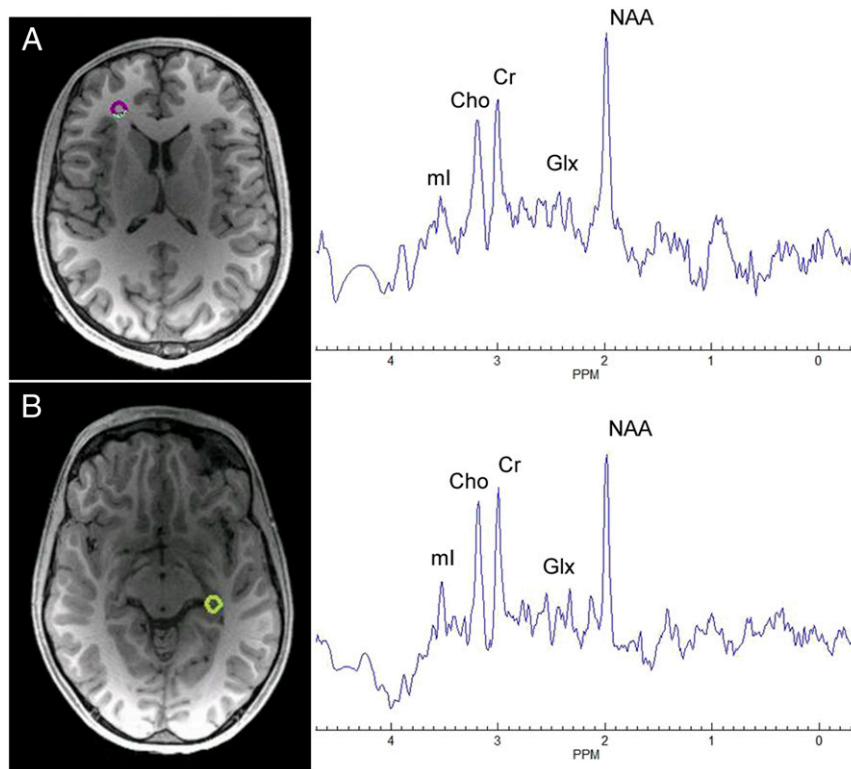
*FDR < 0.05.

Fig. 1. Representative spectra for (*A*) left anterior corona radiata and (*B*) right hippocampus locations.

providing some support for this hypothesis. Furthermore, our mediation analyses support the hypothesis that the levels of NAA, particularly in the white matter and subcortical gray matter regions, mediate the relationship between FCVRS and WMH that represent regions of demyelination, often associated with cerebrovascular factors.

The anatomic pattern of relationship between FCVRS and NAA levels shares some similarities with previous studies of healthy cohorts examining patterns of WMH in relationship to cognition and cardiovascular risk factors. Birdsill and colleagues found cognitive functions—in particular, processing speed—to be associated with WMH volume in the superior and anterior corona radiata and cingulum, independent of age (42). Habes and colleagues found that WMH volume partially mediated the relationships of age and cardiovascular risk factors to patterns of brain atrophy characteristic of both normal aging and Alzheimer's disease; increased WMH load was particularly associated with gray matter atrophy in temporal and frontal lobes, with effects seen for the cingulate and hippocampus as well (6). In the current study, cardiovascular risk factors were prominently related to NAA levels in the anterior and superior corona radiata, cingulum, hippocampus, and cingulate gyrus. This anatomic convergence hints at an overlap of mechanisms linking cardiovascular risk factors to WMH and decreased NAA. Of note also is that, in previous studies, cardiovascular risk factors explained only a modest proportion of variance in WMH burden (6, 43), indicating the contribution of other factors to brain atrophy antecedent to cognitive decline. Underscoring the multifactorial origin of atrophy characteristic of neurodegenerative disease, Schreiner and colleagues found that amyloid-beta burden and WMH independently predicted myo-inositol/NAA ratios in the posterior cingulate cortex of cognitively intact elderly individuals, although they did not find this relationship for white matter myo-inositol/NAA (44).

The findings of an inverse relationship between FCVRS and creatine levels may also reflect a disturbance in brain bioenergetics.

Total creatine quantified with MRS is a combination of creatine and phosphocreatine. Creatine can be derived from diet, hepatic production, or de novo synthesis within the brain. Phosphocreatine is synthesized by a reversible transfer of a phosphate group from ATP and may serve as a transport and buffering vehicle to ensure that ATP can be regenerated when and where it is needed in cells (45). This energetic buffer can protect axons during periods of ischemic-like depletion of ATP production by mitochondria (46). Creatine may also preserve oligodendrocyte viability under inflammatory conditions (47). NAA and creatine levels in the white matter may thus be more vulnerable to increased cardiovascular risks.

The lack of significant findings between FCVRS (after covarying for age and sex) and Glx requires additional consideration. Higher FCVRS was strongly correlated with reduced Glx levels throughout the brain, but these correlations likely represent the strong influence of age on both FCVRS and Glx, as covarying for age greatly attenuated the effects. While decreased Glx has been associated with cognitive impairment and Alzheimer's disease in older samples (17–19), we do not find evidence supporting Glx as a marker of the contribution of cardiovascular risk.

The cross-sectional nature of this study limits interpretation regarding the causal pathways between cardiovascular risk factors and neurochemistry. As MRS cannot distinguish levels of NAA or other metabolites among cell types containing these compounds, we have limited ability to interpret these findings in terms of cellular level mechanisms. The 3D, whole-brain magnetic resonance spectroscopic imaging (MRSI) approach used in this study has the advantage of examining the influence of cardiovascular risk factors on neurochemistry across the brain in a single experiment. However, this approach has limitations, especially regarding limited spatial resolution and sensitivity compared to whole-brain MRSI conducted at higher field strengths. EPSI may be of most value as an anatomically unbiased method of screening to identify regions of highest interest
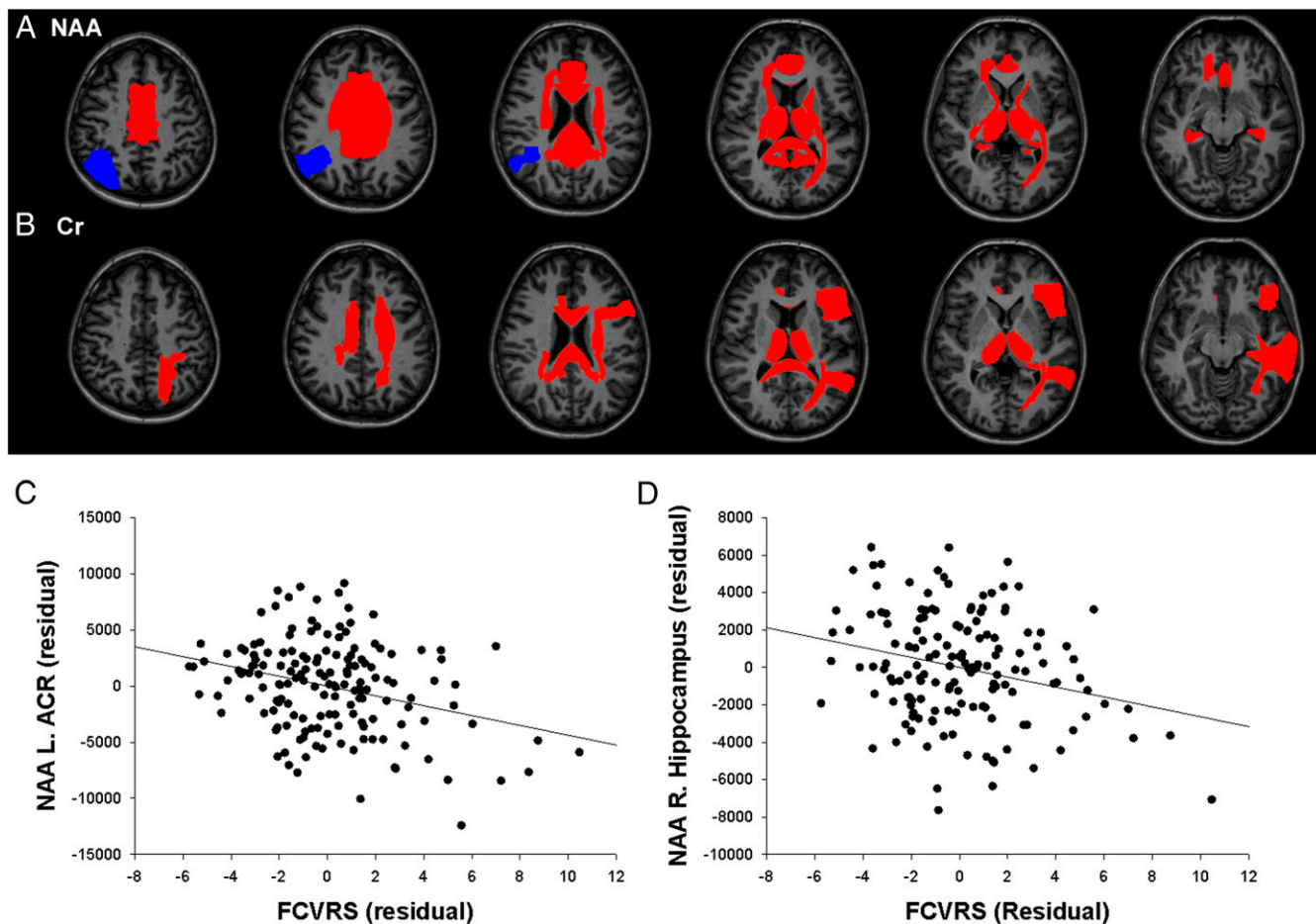
Chiappelli et al.

www.manaraa.com

Fig. 2. Relationship of regional NAA (*A*) and creatine (Cr) (*B*) to FCVRS; regions in red showed inverse correlations between metabolite and FCVRS that were significant after covarying age and sex and accounting for multiple comparisons; regions in blue showed significant positive correlations between metabolite and FCVRS. (*C* and *D*) Two examples, one from white matter and one from gray matter, of the associations between NAA and FCVRS. (*C*) Scatterplot of relationship between FCVRS and NAA in left anterior corona radiata, displaying residuals of both variables after regressing age and sex. (*D*) Scatterplot of relationship between FCVRS and NAA in right hippocampus.

for follow-up studies employing other MRS technologies. Another limitation is that our study was performed in a sample of individuals from a rural population with minimal substance use and formal education levels limited to the eighth grade, possibly limiting the extent to which the current findings can be generalized to the greater population. For example, in our sample only 9.8% of the participants were smokers, compared to 19.3% of the general US population who use tobacco products (48). The limitations of the FCVRS used here to index cardiovascular risk factors must also be noted. The formula for this risk score was based on an empirical study of a predominantly urban/suburban white American sample and may require recalibration for other populations. Furthermore, the FCVRS formula does not include factors that may be particularly relevant to brain aging and risk for cognitive decline, such as genetics, diet, activity levels, or markers of systemic inflammation and/or oxidative stress (49). Obesity is associated with oxidative stress and increased inflammatory tone (50, 51), mechanisms that potentially drive cardiovascular risk and compromise white matter. For example, oxidative stress has been found to be closely related to cardiovascular disease risk factors incorporated in the FCVRS and to independently predict cardiovascular and cerebrovascular illness (51, 52). Similarly, increased inflammatory tone (53, 54) and obesity (7, 55) have been linked to cardiovascular diseases and white matter abnormalities.

Future research should consider incorporating these factors in indices of cardiovascular health risks.

Cardiovascular risk factors are increasingly recognized as contributing to the development of cognitive impairment, neurodegenerative diseases, and dementia. However, the associated mechanisms of pathophysiology are yet to be fully understood. Large-scale clinical trials with intense care focusing on blood pressure showed only marginal effects in reducing dementia or WMH accumulation (56, 57). Other preventative strategies such as use of statins or creatine supplementation have also been largely disappointing in attenuating risk for neurodegenerative disorders (58, 59). Development of more robust preventative strategies may require a more nuanced understanding of the pathways connecting early cardiovascular risks to irreversible brain changes. Here we found that in individuals without significant neurological disturbance, cardiovascular risk factors are related to decreased levels of NAA and creatine, particularly in white matter regions. White matter NAA and creatine may be valuable biomarkers in future mechanistic and intervention studies on the link between common cardiovascular risk factors and neurodegenerative disorders.

Materials and Methods

Participants and Clinical Assessments. Magnetic resonance scanning was completed in 163 OOA/M participants (69 male, 94 female) from Pennsylvania and Maryland (scanned from 2017 to 2018), and EPSI was an add-on study to the ongoing Amish Connectome Project. The average age of

Chiappelli et al.

www.manaraa.com

participants was 39.8 ± SD 17.9 y. The Structured Clinical Interview for DSM-5 was used to identify or rule out psychiatric diagnoses in all participants. Exclusion criteria included history of major medical and neurological conditions, including epilepsy, cerebrovascular accident, head injury with cognitive sequelae, and mental retardation. Participants with unstable or major medical illnesses were excluded, but common medical conditions without current complications such as stable hypertension ($n = 9$) or type II diabetes ($n = 5$) were not excluded. Participants with current major psychiatric disorders such as mood or psychotic disorders were excluded. Participants were screened for tobacco use, and 16 participants were identified as current users. Participants gave written informed consent. The study was approved by the University of Maryland Baltimore Institutional Review Board.

Magnetic Resonance Spectroscopic Imaging. All imaging data were collected on a 3 Tesla Prisma scanner equipped with a 64-channel head coil and a high-performance gradient system. High-resolution T1 MPRAGE (0.8 × 0.8 × 0.8 mm) was obtained on each subject for tissue segmentation and image registration for EPSI. Whole-brain MRSI was acquired with a 3DEPSI sequence (60): repetition time (TR) = 1,550 ms, TE = 17.6 ms, lipid inversion nulling with inversion time = 198 ms, flip angle = 71°, field-of-view: 280 × 280 × 180 mm, 50 × 50 voxels in 18 slices, voxel size = 5.6 × 5.6 × 10 mm, total acquisition time: ~16 min with water and lipid suppression. A water reference MRSI acquisition was interleaved within the metabolite acquisition to be used for phase correction and normalization. Both structural MPRAGE and EPSI were acquired +15° from the anterior commissure–posterior commissure line. EPSI data were processed with the Metabolite Imaging and Data Analysis System (MIDAS) software package (25). Images were reconstructed, corrected for B$_0$ shifts, interpolated to 64 × 64 × 32 points, and spatially smoothed (Gaussian kernel 5 mm in plane, 7 mm through plane), which resulted in an effective voxel volume of ~1.5 mL. Spectral fitting was performed using a common Gaussian line shape for all resonances, and the basis set generated in MIDAS included myo-inositol, creatine-containing compounds (Cre), NAA, choline-containing compounds (Cho), and glutamate and glutamine (Glx) (61). Data quality was assessed, and voxels were excluded if the spectral line width was greater than 13 Hz, the Cre Cramer-Rao lower bounds (CRLB) were greater than 40%, and the Cre confidence limits were greater than 20%. The water resonance was also fit, and voxels were excluded for a water line width greater than 12 Hz, CRLB greater than 2%, confidence limits greater than 20%, and a frequency shift greater than 20 Hz. Additional criteria were a minimum tissue fractional volume of less than 20% and a data value greater than 4 SDs away from the mean for all voxels that passed previously listed criteria. Signal normalization for the individual metabolite maps was carried out using the water MRSI, which was scaled to 100% water equivalence based on information from the tissue segmentation map, which was derived from the T1-weighted MRI using SPM12. Results are presented in institutional units.

All metabolite maps were spatially registered to the "Eve" reference MRI (62), which was mapped to a brain atlas with 107 regions-of-interest. Mean values were generated for each brain region, with voxels excluded from statistical analyses if the spectral line width was less than 2 Hz and greater than 12 Hz, if the voxel value was greater than 3 SDs away from the mean across the viable voxels, and if the proportion of CSF within the voxel was greater than 30%. All EPSI voxels from each cortical and subcortical gray matter region of the atlas (62) were averaged to represent the level of the metabolite in that region, resulting in a map representing the distribution of each metabolite by region across the brain. However, regions for which >10% of participants had voxels rejected due to failure to pass the above quality assurance procedure were excluded from analysis, leaving 48 gray matter and 21 white matter regions (n of regions = 69; see Table 1 for retained regions).

Fluid-Attenuated Inversion Recovery MRI. We used a semiautomated analysis pipeline to quantify the volume and count of WMH. The pipeline uses coregistered high-resolution (0.8 × 0.8 × 0.8 mm) T1 and T2w 3D sequences similar to the approach used by the Human Connectome Project (http://www.humanconnectomeproject.org). The WMH burden is quantified as the combined (ependymal + subcortical) WMH volume (mm^3) and the number of subcortical WMH regions (63, 64). See *SI Appendix* for further details.

FCVRS. Based on empirical data from the Framingham Heart Study, the FCVRS is a sex-specific multivariable algorithm based on common laboratory measures and risk factors used to predict an individual's risk for cardiovascular diseases such as heart failure, stroke, and coronary artery disease (32). The score incorporates age, plasma levels of high-density lipoprotein and total cholesterol, diagnosis of type II diabetes, smoking status, and systolic blood pressure (points calculated differently depending on whether being treated with antihypertensive or not), with different scoring for men and women. The FCVRS has previously been found to be predictive of cognitive decline and WMH in healthy elderly individuals (4, 6).

Statistics. As age and sex are factored into the FCVRS (32) and may be related to metabolite levels, all analyses were examined by linear regression models including age and sex as covariates. For each metabolite, multiple comparisons for the number of regions ($n = 69$) were corrected for using the Benjamini–Hochberg method, with an FDR of 0.05 (65). The key metabolites found to be related to FCVRS were further explored in their relationships with specific subcomponents of the FCVRS following the same pattern. To test if observed relationships between FCVRS and NAA levels had implications for white matter changes, we conducted mediation analyses to test models using age-regressed FCVRS as an independent variable, NAA levels as a mediator, and WMH as a dependent variable, with age and sex as covariates (*SI Appendix*, Fig. S1). In these models, 3 summary measures of NAA were used: average NAA across all white matter regions; average NAA across cortical gray matter regions; and average NAA across subcortical gray matter regions. Two global WMH measures were used: log-transformed total lesion volume and total lesion number. The quasi-Bayesian Monte Carlo method was used for statistical inference (66).

1. R. Aljondi, C. Szoeke, C. Steward, A. Gorelik, P. Desmond, The effect of midlife cardiovascular risk factors on white matter hyperintensity volume and cognition two decades later in normal ageing women. *Brain Imaging Behav.*, 10.1007/s11682-018-9970-5 (2018).

2. R. F. Gottesman *et al.*, Association between midlife vascular risk factors and estimated brain amyloid deposition. *J. Am. Med. Assoc.* **317**, 1443–1450 (2017).

3. M. P. Pase *et al.*, Association of aortic stiffness with cognition and brain aging in young and middle-aged adults: The Framingham third generation cohort study. *Hypertension* **67**, 513–519 (2016).

4. J. S. Rabin *et al.*, Interactive associations of vascular risk and β-amyloid burden with cognitive decline in clinically normal elderly individuals: Findings from the Harvard aging brain study. *JAMA Neurol.* **75**, 1124–1131 (2018).

5. W. Williamson *et al.*, Association of cardiovascular risk factors with MRI indices of cerebrovascular structure and function and white matter hyperintensities in young adults. *J. Am. Med. Assoc.* **320**, 665–673 (2018).

6. M. Habes *et al.*, White matter hyperintensities and imaging patterns of brain ageing in the general population. *Brain* **139**, 1164–1179 (2016).

7. M. Ryan *et al.*, Lipid metabolism, abdominal adiposity, and cerebral health in the amish. *Obesity (Silver Spring)* **25**, 1876–1880 (2017).

8. J. R. Moffett, B. Ross, P. Arun, C. N. Madhavarao, A. M. Namboodiri, N-acetylaspartate in the CNS: From neurodiagnostics to neurobiology. *Prog. Neurobiol.* **81**, 89–131 (2007).

9. C. D. Rae, A guide to the metabolic pathways and function of metabolites observed in human brain 1H magnetic resonance spectra. *Neurochem. Res.* **39**, 1–36 (2014).

10. A. Horská *et al.*, In vivo quantitative proton MRSI study of brain development from childhood to adolescence. *J. Magn. Reson. Imaging* **15**, 137–143 (2002).

11. M. H. Baslow, N-acetylaspartate in the vertebrate brain: Metabolism and function. *Neurochem. Res.* **28**, 941–953 (2003).

12. G. Chakraborty, P. Mekala, D. Yahya, G. Wu, R. W. Ledeen, Intraneuronal N-acetylaspartate supplies acetyl groups for myelin lipid synthesis: Evidence for myelin-associated aspartoacylase. *J. Neurochem.* **78**, 736–745 (2001).

13. E. Joe, L. D. Medina, J. M. Ringman, J. O'Neill, 1H MRS spectroscopy in preclinical autosomal dominant Alzheimer disease. *Brain Imaging Behav.* **13**, 925–932 (2019).

14. M. Marjanska *et al.*, Monitoring disease progression in transgenic mouse models of Alzheimer's disease with proton magnetic resonance spectroscopy. *Proc. Natl. Acad. Sci. U.S.A.* **102**, 11906–11910 (2005).

15. P. J. Modrego, N. Fayed, M. Sarasa, Magnetic resonance spectroscopy in the prediction of early conversion from amnestic mild cognitive impairment to dementia: A prospective cohort study. *BMJ Open* **1**, e000007 (2011).

16. N. R. Sibson *et al.*, Stoichiometric coupling of brain glucose metabolism and glutamatergic neuronal activity. *Proc. Natl. Acad. Sci. U.S.A.* **95**, 316–321 (1998).

17. N. Fayed, P. J. Modrego, G. Rojas-Salinas, K. Aguilar, Brain glutamate levels are decreased in Alzheimer's disease: A magnetic resonance spectroscopy study. *Am. J. Alzheimers Dis. Other Demen.* **26**, 450–456 (2011).

18. D. Huang *et al.*, Glutamate-glutamine and GABA in brain of normal aged and patients with cognitive impairment. *Eur. Radiol.* **27**, 2698–2705 (2017).

www.manaraa.com

19. G. Oeltzschner et al., Neurometabolites and associations with cognitive deficits in mild cognitive impairment: A magnetic resonance spectroscopy study at 7 Tesla. Neurobiol. Aging 73, 211–218 (2019).

20. M. M. Gonzales et al., Aerobic fitness and the brain: Increased N-acetyl-aspartate and choline concentrations in endurance-trained middle-aged adults. Brain Topogr. 26, 126–134 (2013).

21. S. Gazdzinski et al., BMI and neuronal integrity in healthy, cognitively normal elderly: A proton magnetic resonance spectroscopy study. Obesity (Silver Spring) 18, 743–748 (2010).

22. T. C. Durazzo et al., Chronic cigarette smoking in healthy middle-aged individuals is associated with decreased regional brain N-acetylaspartate and glutamate levels. Biol. Psychiatry 79, 481–488 (2016).

23. M. Z. Goryawala, S. Sheriff, A. A. Maudsley, Regional distributions of brain glutamate and glutamine in normal subjects. NMR Biomed. 29, 1108–1116 (2016).

24. A. A. Maudsley et al., Comprehensive processing, display and analysis for in vivo MR spectroscopic imaging. NMR Biomed. 19, 492–503 (2006).

25. A. A. Maudsley et al., Mapping of brain metabolite distributions by volumetric proton MR spectroscopic imaging (MRSI). Magn. Reson. Med. 61, 548–559 (2009).

26. A. A. Maudsley, C. Domenig, S. Sheriff, Reproducibility of serial whole-brain MR spectroscopic imaging. NMR Biomed. 23, 251–256 (2010).

27. H. Zhu, P. B. Barker, MR spectroscopy and spectroscopic imaging of the brain. Methods Mol. Biol. 711, 203–226 (2011).

28. O. Al-Iedani, J. Lechner-Scott, K. Ribbons, S. Ramadan, Fast magnetic resonance spectroscopic imaging techniques in human brain- applications in multiple sclerosis. J. Biomed. Sci. 24, 17 (2017).

29. X. Q. Ding et al., Reproducibility and reliability of short-TE whole-brain MR spectroscopic imaging of human brain at 3T. Magn. Reson. Med. 73, 921–928 (2015).

30. Y. Zhang et al., Comparison of reproducibility of single voxel spectroscopy and whole-brain magnetic resonance spectroscopy imaging at 3T. NMR Biomed. 31, e3898 (2018).

31. H. Maghsudi et al., Regional metabolite concentrations in aging human brain: Comparison of short-TE whole brain MR spectroscopic imaging and single voxel spectroscopy at 3T. Clin. Neuroradiol., 10.1007/s00062-018-00757-x (2019).

32. R. B. D'Agostino, Sr et al., General cardiovascular risk profile for use in primary care: The Framingham heart study. Circulation 117, 743–753 (2008).

33. J. A. Fuchs, R. M. Levinson, R. R. Stoddard, M. E. Mullet, D. H. Jones, Health risk factors among the Amish: Results of a survey. Health Educ. Q. 17, 197–211 (1990).

34. J. M. Dietschy, S. D. Turley, Cholesterol metabolism in the brain. Curr. Opin. Lipidol. 12, 105–112 (2001).

35. U. Wisløff et al., Cardiovascular risk factors emerge after artificial selection for low aerobic capacity. Science 307, 418–420 (2005).

36. A. Eirin, A. Lerman, L. O. Lerman, Mitochondrial injury and dysfunction in hypertension-induced cardiac damage. Eur. Heart J. 35, 3258–3266 (2014).

37. R. J. Webber, J. Edmond, The in vivo utilization of acetoacetate, D-(-)-3-hydroxybutyrate, and glucose for lipid synthesis in brain in the 18-day-old rat. Evidence for an acetyl-CoA bypass for sterol synthesis. J. Biol. Chem. 254, 3912–3920 (1979).

38. M. Lopes-Cardozo, J. W. Koper, W. Klein, L. M. Van Golde, Acetoacetate is a cholesterogenic precursor for myelinating rat brain and spinal cord. Incorporation of label from [3-14C]acetoacetate, [14C]glucose and 3H2O. Biochim. Biophys. Acta 794, 350–352 (1984).

39. Y. Assaf et al., White matter changes in multiple sclerosis: Correlation of q-space diffusion MRI and 1H MRS. Magn. Reson. Imaging 23, 703–710 (2005).

40. S. A. Wijtenburg et al., Relationship between fractional anisotropy of cerebral white matter and metabolite concentrations measured using (1)H magnetic resonance spectroscopy in healthy adults. Neuroimage 66, 161–168 (2013).

41. J. Chiappelli et al., Alterations in frontal white matter neurochemistry and microstructure in schizophrenia: Implications for neuroinflammation. Transl. Psychiatry 5, e548 (2015).

42. A. C. Birdsill et al., Regional white matter hyperintensities: Aging, Alzheimer's disease risk, and cognitive function. Neurobiol. Aging 35, 769–776 (2014).

43. J. M. Wardlaw et al., Vascular risk factors, large-artery atheroma, and brain white matter hyperintensities. Neurology 82, 1331–1338 (2014).

44. S. J. Schreiner et al., Brain amyloid burden and cerebrovascular disease are synergistically associated with neurometabolism in cognitively unimpaired older adults. Neurobiol. Aging 63, 152–161 (2018).

45. R. H. Andres, A. D. Ducray, U. Schlattner, T. Wallimann, H. R. Widmer, Functions and effects of creatine in the central nervous system. Brain Res. Bull. 76, 329–343 (2008).

46. H. Shen, M. P. Goldberg, Creatine pretreatment protects cortical axons from energy depletion in vitro. Neurobiol. Dis. 47, 184–193 (2012).

47. K. A. Chamberlain, K. S. Chapey, S. E. Nanescu, J. K. Huang, Creatine enhances mitochondrial-mediated oligodendrocyte survival after demyelinating injury. J. Neurosci. 37, 1479–1492 (2017).

48. T. W. Wang et al., Tobacco product use among adults: United States, 2017. MMWR Morb. Mortal. Wkly. Rep. 67, 1225–1232 (2018).

49. M. Wang, J. E. Norman, V. J. Srinivasan, J. C. Rutledge, Metabolic, inflammatory, and microvascular determinants of white matter disease and cognitive decline. Am. J. Neurodegener. Dis. 5, 171–177 (2016).

50. F. Santilli, M. T. Guagnano, N. Vazzana, S. La Barba, G. Davi, Oxidative stress drivers and modulators in obesity and cardiovascular disease: From biomarkers to therapeutic approach. Curr. Med. Chem. 22, 582–595 (2015).

51. J. F. Keaney, Jr et al.; Framingham Study, Obesity and systemic oxidative stress: Clinical correlates of oxidative stress in the Framingham study. Arterioscler. Thromb. Vasc. Biol. 23, 434–439 (2003).

52. Y. Xuan, X. Gào, B. Holleczek, H. Brenner, B. Schöttker, Prediction of myocardial infarction, stroke and cardiovascular mortality with urinary biomarkers of oxidative stress: Results from a large cohort study. Int. J. Cardiol. 273, 223–229 (2018).

53. G. A. Rosenberg, Inflammation and white matter damage in vascular cognitive impairment. Stroke 40 (suppl. 3), S20–S23 (2009).

54. D. Kaiser et al., Spontaneous white matter damage, cognitive decline and neuroinflammation in middle-aged hypertensive rats: An animal model of early-stage cerebral small vessel disease. Acta Neuropathol. Commun. 2, 169 (2014).

55. S. Kullmann et al., Specific white matter tissue microstructure changes associated with obesity. Neuroimage 125, 36–44 (2016).

56. J. W. van Dalen et al., Effect of long-term vascular care on progression of cerebrovascular lesions: Magnetic resonance imaging substudy of the PreDIVA trial (prevention of dementia by intensive vascular care). Stroke 48, 1842–1848 (2017).

57. J. D. Williamson et al.; SPRINT MIND Investigators for the SPRINT Research Group, Effect of intensive vs standard blood pressure control on probable dementia: A randomized clinical trial. J. Am. Med. Assoc. 321, 553–561 (2019).

58. W. G. Wood, L. Li, W. E. Müller, G. P. Eckert, Cholesterol as a causative factor in Alzheimer's disease: A debatable hypothesis. J. Neurochem. 129, 559–572 (2014).

59. A. Bender, T. Klopstock, Creatine for neuroprotection in neurodegenerative disease: End of story? Amino Acids 48, 1929–1940 (2016).

60. A. Ebel, A. A. Maudsley, Improved spectral quality for 3D MR spectroscopic imaging using a high spatial resolution acquisition strategy. Magn. Reson. Imaging 21, 113–120 (2003).

61. B. J. Soher, K. Young, V. Govindaraju, A. A. Maudsley, Automated spectral analysis III: Application to in vivo proton MR spectroscopy and spectroscopic imaging. Magn. Reson. Med. 40, 822–831 (1998).

62. K. Oishi et al., Atlas-based whole brain white matter analysis using large deformation diffeomorphic metric mapping: Application to normal elderly and Alzheimer's disease participants. Neuroimage 46, 486–499 (2009).

63. P. Kochunov et al., Analysis of genetic variability and whole genome linkage of whole-brain, subcortical, and ependymal hyperintense white matter volume. Stroke 40, 3685–3690 (2009).

64. P. Kochunov et al., Whole brain and regional hyperintense white matter volume and blood pressure: Overlap of genetic loci produced by bivariate, whole-genome linkage analyses. Stroke 41, 2137–2142 (2010).

65. Y. Benjamini, Y. Hochberg, Controlling the false discovery rate: A practical and powerful approach to multiple testing. J. R. Stat. Soc. B 57, 289–300 (1995).

66. D. Tingley, T. Yamamoto, K. Hirose, L. Keele, K. Imai, Mediation: R Package for Causal Mediation Analysis (UCLA Statistics/American Statistical Association, 2014).

Chiappelli et al.

www.manaraa.com